pH Dependence of Arsenic Oxidation by Rice-Husk-Derived Biochar: Roles of Redox-Active Moieties

Delai Zhong,[†,‡] Yi Jiang,[‡] Zezhou Zhao,[†] Linling Wang,[*,†] Jing Chen,[†] Shupeng Ren,[†] Zhenhua Liu,[†] Yanrong Zhang,[†,*] Daniel C.W. Tsang,[‡] and John C. Crittenden[§]

[†]School of Environmental Science and Engineering, Huazhong University of Science and Technology, Wuhan, 430074, P.R. China

[‡]Department of Civil and Environmental Engineering, The Hong Kong Polytechnic University, Hung Hom, Kowloon, Hong Kong, P.R. China

[§]Brook Byers Institute of Sustainable Systems and School of Civil and Environmental Engineering, Georgia Institute of Technology, Atlanta, GA 30332, United States

ABSTRACT

Biochars have demonstrated great potential for water decontamination and soil remediation, however, their redox reactivity toward trace contaminants and the corresponding redox-active moieties (RAMs, i.e., phenolic –OH, semiquinone-type persistent free radicals (PFRs), and quinoid C=O) remain poorly understood. Here we investigated the roles of the RAMs on biochar in oxidation of As(III) under varying pH and O_2 conditions. The results showed that the promoted oxidation of As(III) by the RAMs is strongly pH dependent. Under acidic and neutral conditions, only the oxidation of As(III) by •OH and H_2O_2 produced from activation of O_2 by phenolic –OH and semiquinone-type PFRs occurred. In contrast, the oxidation by semiquinone-type PFRs, quinoid C=O, and H_2O_2 (if O_2 was introduced) appeared under alkaline conditions. This pH-dependent oxidation behavior was attributed to the varying redox activities of RAMs, as confirmed by multiple characterization and validation experiments using biochar with tuned RAMs compositions, as well as thermodynamics evaluation. Our findings provide new insights into the roles of the RAMs on biochar in the promoted oxidation of trace As(III) over a broader pH range under both anoxic and oxic conditions. This study also paves a promising way to oxidize As(III) with biochar.

INTRODUCTION

Biochar, as a pyrogenic carbonaceous material, has been the subject of considerable research for wide applications in environmental remediation,[1,2] agricultural application,[3] and mitigation of global climate change[4] due to its unique properties (e.g., porous structure, number of oxygen-containing functional groups, and abundant nutrients). For example, biochar has been increasingly applied to decontaminate both water and soil systems from heavy metals and organic contaminants. The mechanisms of heavy metal decontamination generally involve complexation with surface oxygen-containing functional groups on biochar,[5] chemical precipitation with inherent minerals from biochar,[2] ions exchange,[1] and electrostatic interaction,[6] etc. While the process is typically associated with partitioning[7] and adsorption via π^{+}–π interaction[8,9] and/or hydrogen bonding with respect to the removal of organic pollutants.[10]

Recently, the role of the redox reactivity of biochar in contaminant removal has been increasingly noticed. For instance, Zhou and his coworkers found that biochar could generate reactive oxygen species (ROS), especially hydroxyl free radical (•OH) for degradation of organic contaminant, via the activation of hydrogen peroxide (H_2O_2) and molecular oxygen (O_2).[11,12] They attributed the reactions to the presence of solid-phase free radicals (SFRs) that could trigger a successive single-electron transfer reaction for •OH formation. These SFRs are typically unpaired π-electrons delocalized over the aromatic rings of biochar. More importantly, these SFRs possess reactivity with long half-lives ranging from hours to days in the ambient environment, thus being defined as persistent free radicals (PFRs).[13,14] Meanwhile, Pan's group further demonstrated

that PFRs on biochar could reductively degrade *p*-nitrophenol, in addition to the indirect oxidative degradation by •OH that was produced from a traditional Fenton-like reaction of PFRs.[13,15] The reductive capacity of the PFRs on biochar was also demonstrated in our recent study on reductive adsorption of Cr(VI).[6] In contrast, Dong et al. discovered that PFRs on dissolved organic matter (DOM) released from biochar directly enabled As(III) oxidation, as evidenced by electron spin resonance (ESR) results.[16] In addition to PFRs, other redox-active moieties (RAMs, e.g., phenolic –OH and quinoid C=O moieties) may participate in redox transformations of contaminants. Subsequently, Pan and his colleagues further proposed that phenolic –OH on biochar were mainly responsible for *p*-nitrophenol reduction, in addition to the PFRs.[13] Moreover, phenolic –OH and quinoid C=O on biochar were found to promote microbial redox transformations of contaminants (e.g., acetate, and nitrate).[17] A "geobattery" mechanism was proposed, suggesting that phenolic –OH and quinoid C=O donated and accepted electrons respectively in the microbial redox reactions. To date, these studies primarily focus on the individual roles of PFRs or quinone moieties (i.e., phenolic –OH and quinoid C=O) in the redox transformations of contaminants at circumneutral pH. However, little information is available on their overall roles and relative significance in redox transformation of inorganic contaminants over a broad and environmentally relevant pH range, especially varying from acidic to alkaline conditions.

The solution pH plays a crucial role in determining the extent and pathway of redox reactions between RAMs on carbon-based materials (e.g., humic substances (HS) and biochar-derived DOM) and redox-sensitive contaminants such as arsenic (As).[16,18-20]

As occurs predominantly as inorganic arsenite (As(III)) and arsenate (As(V)) in environmental media. Considering the higher toxicity and mobility of As(III) than As(V), the oxidation of As(III) to As(V) is generally employed for enhancing the removal of As.[21] The transformation of As(III) to As(V) is significantly dependent on the solution pH.[18,20] For example, Jiang et al. showed that a model HS quinone (9,10-anthraquinone-2,6-disulfonic acid, AQDS) could oxidize 0.5%, 12.6%, and 67.3% of As(III) at pH 3.0, 7.0, and 11.0 under anoxic conditions, respectively. PFRs on AQDS were suggested to directly oxidize As(III) at pH values of 3.0 to 11.0 in anoxic solutions.[18] Recently, Qin et al. reported that hydroquinone enabled 33–92% of As(III) oxidation and 1,4-benzoquinone oxidized 0–80% of As(III) with the pH increasing from 6.5 to 8.5.[19] They proposed that PFRs generated *in situ* from both hydroquinone and 1,4-benzoquinone directly oxidized As(III) and mediated ROS generation for subsequent As(III) oxidation. These studies imply that the RAMs associated with carbon-based materials such as biochar may have similar pH-dependent redox reactivity. Compared to HS, biochar possesses a smaller amount of oxygen-containing RAMs (e.g., quinoid C=O) and lower water solubility, but higher conductivity (development of graphitic structure) and porosity, due to the differences in their elemental compositions and formation pathways.[6,22-24] Therefore, RAMs on biochar are envisioned to play pH-dependent and multiple roles in As(III) oxidation, which might be potentially different from those on HS. In the biochar-arsenic system, there have been only a few studies on As(III) oxidation by biochar over a wide pH range,[16,25,26] and the reactions between biochar and As(III), especially the underlying roles and

relative significance of RAMs on biochar under acidic to alkaline pH conditions, are still not well understood.

Herein, we investigated As(III) oxidation by rice-husk-derived biochar over a wide pH range of 3.0–9.5 under both anoxic and oxic conditions.[27-30] Electron paramagnetic resonance (EPR), Fourier transform infrared (FTIR) spectroscopy, X-ray photoelectron spectroscopy (XPS), and Boehm titration analyses were applied to decipher the underlying roles of RAMs in As(III) oxidation. More importantly, the RAM compositions of biochar were tuned with oxidation, reduction and thermal treatments to elucidate the subsequent As(III) oxidation behavior, consolidating their redox roles. In addition, potential thermodynamics were approximately evaluated to illustrate the significance of pH-dependent As(III) oxidation by biochar. Based on our experimental observations, the mechanisms of As(III) oxidation by biochar RAMs were proposed.

MATERIALS AND METHODS

Materials and Chemicals. Rice husk (RH) was collected from a farm located in Hubei province, central China. Prior to pyrolysis, the RH was washed by deionized water (18.2 MΩ cm) and air-dried at room temperature for several days. $NaAsO_2$ (99%) and $Na_2HAsO_4 \cdot 7H_2O$ (99%) were obtained from Sigma-Aldrich and used for the preparation of As(III) and As(V) solutions, respectively. Other materials and chemicals used in this study are described in Text S1 of Supporting Information (SI).

Biochar Production and Characterization. Biochar samples were produced under controlled conditions in the laboratory using O_2-limited pyrolysis of RH. Pyrolysis temperature and duration time were 400 °C and 1 h, respectively. To avoid the effect

of DOM released from biochar on As(III) oxidation experiments,[16] the obtained biochar was washed repeatedly with deionized water until the total organic carbon in the supernatant was less than 0.1 mg C/L. The resulting solid particles were then dried under vacuum at 60 °C for 24 h, and grounded to pass through a 0.149-mm sieve. They were labeled as BC400 according to the pyrolysis temperature, and stored at 4 °C in the dark for later use. The biochar sample was freshly and regularly prepared due to the natural attenuation of RAMs on biochar with time.[13]

To further verify the roles of RAMs, i.e., phenolic –OH, semiquinone-type PFRs, and quinoid C=O in the As(III) oxidation, a series of BC400 pretreatments were conducted to tune its RAM compositions. It has been reported that borohydride can reduce oxidized functional groups (OFGs, e.g., quinoid C=O and PFRs) into reduced functional groups (RFGs, e.g., phenolic –OH and semiquinone-type PFRs).[31] Conversely, H_2O_2 treatment could transform the RFGs into the OFGs.[32] Herein, we employed KBH_4 and H_2O_2 to tune these three moieties on biochar. Typically, each 10 g sample of BC400 was dispersed in 500 mL 5 wt.% KBH_4 or H_2O_2 solutions in a brown conical flask. The mixture was then magnetically stirred for 24 h at either 25 or 60 °C. Finally, the suspension was filtered on a vacuum suction filter, thoroughly washed with deionized water and dried under vacuum at 60 °C for 24 h. The obtained products were noted as oBC400 and rBC400, respectively. Details of the preparation of rBC400 and oBC400 can be found in Text S2 of SI. Additionally, we prepared BC500 by pyrolysis of BC400 at 500 ℃ for 1 h to increase the generation of PFRs on biochar. This was because an elevated pyrolysis temperature varying from 400 to 500 ℃ could

141 remarkably facilitate the generation of PFRs on biochar.[33] To eliminate the RAMs on
142 biochar, BC400 was thermally treated at 800 ℃ for 1 h.[32] The sample collected from
143 this process was denoted as BC800.

144 The elemental C, N, O, and H contents of biochars were characterized by elemental
145 analysis (Vario Micro cube, Elementar, Germany) (Table S1). The FTIR spectra of
146 biochar samples were collected by a VERTEX 80 FTIR spectrometer (Bruker,
147 Germany) with a resolution of 4 cm^{-1} in the region of 400–4000 cm^{-1} (Text S3). PFRs
148 on biochar samples were detected by an electron paramagnetic resonance (EPR)
149 spectrometer with a single cavity (EMX nano, Bruker, Germany) at room temperature,
150 as described in our previous work (Text S4).[6] X-ray photoelectron spectroscopy (XPS)
151 was applied to check oxygen-containing components on the surface of biochar samples
152 (Axis-Ultra DLD-600W, Shimadzu-Kratos, Japan) (Text S5). The modified Boehm
153 titration analysis was conducted to determine phenolic –OH (Text S6).[34]

154 **As(III) Oxidation Experiments.** All batch experiments were performed in
155 magnetically stirred reactors (250 mL) covered with aluminum foil to avoid any
156 photochemical reactions at room temperature. In a typical test, each 0.5 g of biochar
157 powder was dispersed into 250 mL As(III) solution (750 μg/L). During the whole
158 reaction, the suspension pH was maintained at a desired value (i.e., 3.0, 7.0 or 9.5±0.1)
159 by adding 0.1 or 1 M HCl and/or NaOH aqueous solutions when necessary. Anoxic
160 reactions were first performed. To ensure strictly anoxic conditions, all solutions were
161 purged with ultrapure nitrogen for at least 2 h before the anoxic reactions, and the
162 biochar samples were deoxygenated under vacuum for at least 2 h. During the test

periods, the suspension was purged with ultrapure nitrogen to create O_2-free conditions (dissolved oxygen (DO) concentration below 0.2 mg/L). Oxic reactions were carried out in a wide-mouth reactor by exposing the suspension to air with magnetic stirring. During the oxic reactions, the DO concentration was maintained at 8.6 ± 0.2 mg/L as measured by a DO probe (WTW Multi 3410 Multiparameter Meter, Germany). Control experiments without biochar samples were performed under the same conditions described above. At predetermined time intervals (0–24 h), each 2 mL reaction suspension was sampled into 5 drops of methanol (A pretest has demonstrated that excess methanol has a significant interference with As analysis (data not shown)) and rigorously shaken, thus quenching further reaction between •OH and As(III). Then, the sample was immediately filtered through a 0.22-μm filtration membrane for As analysis. During the As(III) oxidation experiments, total As adsorption was negligible (Figure S1 and Text S7); thus, As adsorption behavior was not considered in the following studies. All the experiments were performed in triplicates.

Analytical Methods. As(III) and As(V) in solution were determined by a hydride generation-atomic fluorescence spectrometer (HG-AFS, SA7800, Beijing Bohui Innovation Optoelectronic Technology Co., Ltd.) equipped with a high-performance liquid chromatography (HPLC, LC-100^{PLUS}, Shanghai Wufeng Scientific Instrument Co., Ltd.). A Hamilton PRP-X100 anion-exchange column (10 μm, 4.1×250 mm) was used to separate the As(III) and As(V) species in solution. The detection limits of As(III) and As(V) were 0.15 and 0.3 μg/L, respectively. The total As was obtained from the sum of As(III) and As(V).

The production of H_2O_2 in biochar systems under oxic condition was measured according to a modified DPD method.[35] The production of •OH from biochar oxidation was characterized by EPR coupled with 5,5-dimethyl-1-pyrroline-N-oxide (DMPO) as a spin-trapping agent. Briefly, each 2 g/L biochar suspension with 100 mM DMPO was freshly prepared to initiate the oxic reactions at pH 3.0, 7.0, and 9.5, and the collected supernatant of the mixture was measured on an EPR spectrometer. To further quantify •OH generation, the As(III)-containing solution was replaced by 10 mM benzoic acid (•OH probe) solution and the test was performed in the same scenarios as those of the As(III) oxidation experiments.[32] The cumulative •OH concentration was acquired by measuring *p*-HBA on an Agilent Technologies 1260 Infinity II equipped with a UV detector and an Eclipse XDB-C18 column (5 μm, 4.6×150 mm) based on previous reports.[36] The detection limit of •OH was 0.59 μM. Total organic pollutants released from biochar during the As(III) oxidation were evaluated by a TOC analyzer (TOC-L CPH, Shimadzu).

RESULTS AND DISCUSSION

Effect of pH on As(III) Oxidation and Generation of Reactive Oxygen Species. We investigated As(III) oxidation in biochar/As(III) systems under varying pH (i.e., 3.0, 7.0, and 9.5) and O_2 (i.e., anoxic and oxic) conditions. No As(III) oxidation occurred in the absence of O_2 at pH 3.0 and 7.0, and 39.9% (pH 3.0) and 19.3% (pH 7.0) of As(III) were oxidized within 24 h with subsequent O_2 introduction (Figure 1a and 1b). At pH 9.5, As(III) was completely oxidized after 12 h under anoxic conditions, compared to only 4 h under oxic conditions. The control experiment in the absence of biochar

showed that no As(III) oxidation by O_2 occurred under all pH conditions, except for pH 9.5 (with 21.0% of As(III) being oxidized after 24 h). This was due to the higher reduction potential (Eh) ($E_{pH=9.5}(O_2/•HO_2)$ = –0.127 V) of $O_2/•HO_2$ couple than that ($E_{pH=9.5}$(As(V)/As(III)) = –0.397 V) of As(V)/As(III) couple (Figure 1c). The results suggested that both biochar and O_2 played decisive roles in the As(III) oxidation. The pH- and O_2-dependent As(III) oxidation by biochar was probably related to the Eh values of the As(V)/As(III) couple and other redox couples (e.g., semiquinone PFRs/phenolic –OH couple) on biochar, as well as the $O_2/•HO_2$ couple, which may resemble the observation of As(III) oxidation by HS.[18] The As(III) oxidation by biochar obeyed pseudo first-order kinetics, and the results are listed in Table S2. The fitted k_{obs} values for the As(III) oxidation under oxic conditions were 1.402×10^{-1} h^{-1} at pH 3.0, 0.513×10^{-1} h^{-1} at pH 7.0, and 3.817×10^{-1} h^{-1} at pH 9.5, respectively, which were at least 1.8-fold higher than those at the corresponding pH values (0 h^{-1} at pH 3.0 and 7.0, and 2.161×10^{-1} h^{-1} at pH 9.5, respectively) under anoxic conditions. These observations indicated that O_2 significantly accelerated As(III) oxidation by biochar. Previous studies have documented that biochar can induce the generation of ROS via a successive single-electron transfer reaction for degradation of organic pollutant in oxic solution.[12,32] Thus, we speculated that O_2 might be activated by biochar to produce ROS, especially H_2O_2 and •OH for the promotion of As(III) oxidation.

To verify this, we thus examined the production of H_2O_2 and •OH in the As-free/biochar suspensions under oxic conditions. As depicted in Figure 1d, the cumulative concentration of H_2O_2 slightly occurred at pH 3.0 (a maximum value, 1.0

μM) and pH 7.0 (a maximum value, 4.2 μM), while the cumulative concentration significantly elevated from 0 to 78.8 μM within 24 h at pH 9.5. However, an opposite pattern was found for the production of •OH (Figure 1e), which was further supported by our EPR results (Figure S2). Using EPR with DMPO as a spin-trapping agent, we failed to detect characteristic pattern of DMPO-O_2 adduct, which was likely attributed to the fast dismutation of superoxide anion free radical ($•O_2^-$) and the instability of DMPO-O_2 adduct in the aquatic media.[12,37] Based on the aforementioned literatures and our observations, we proposed that biochar could donate electrons to dissolved O_2 to produce $•O_2^-$, then further accepted an electron or dismutated to form H_2O_2 in the pH range of 3.0 to 9.5. The newly produced H_2O_2 in biochar systems could quickly convert to •OH via a single-electron transfer reaction at pH 3.0 and 7.0, but less likely at pH 9.5. This was possibly related to pH-dependent activation of H_2O_2 by biochar and the promotion of •OH generation by biochar at a lower pH value. Subsequently, the roles of •OH and H_2O_2 in the As(III) oxidation were investigated by performing a series of quenching experiments (i.e., ethanol for •OH and CAT for H_2O_2). The addition of ethanol (which led to the absence of •OH) almost completely quenched the As(III) oxidation at pH 3.0 and 7.0, but had little effect on the As(III) oxidation at pH 9.5 (Figure 1f). In contrast, the addition of CAT (which resulted in both the absence of •OH and H_2O_2) thoroughly quenched the As(III) oxidation at pH 3.0 and 7.0, but partly slowed the As(III) oxidation rate under oxic conditions which was approximately equal to that under anoxic conditions at pH 9.5. These results indicated that •OH was primarily responsible for the As(III) oxidation at pH 3.0 and 7.0, whereas both H_2O_2

and biochar played dominant roles in the As(III) oxidation at pH 9.5 under oxic conditions. In addition, the newly produced H_2O_2 could participate in the direct oxidation of As(III) in biochar systems, which was further confirmed by an additional experiment that the introduction of H_2O_2 directly contributed to As(III) oxidation (Figure S3). Hence, we concluded that biochar could induce the generation of ROS, especially H_2O_2 and •OH, via activation of O_2, resulting in the promotion of the As(III) oxidation.

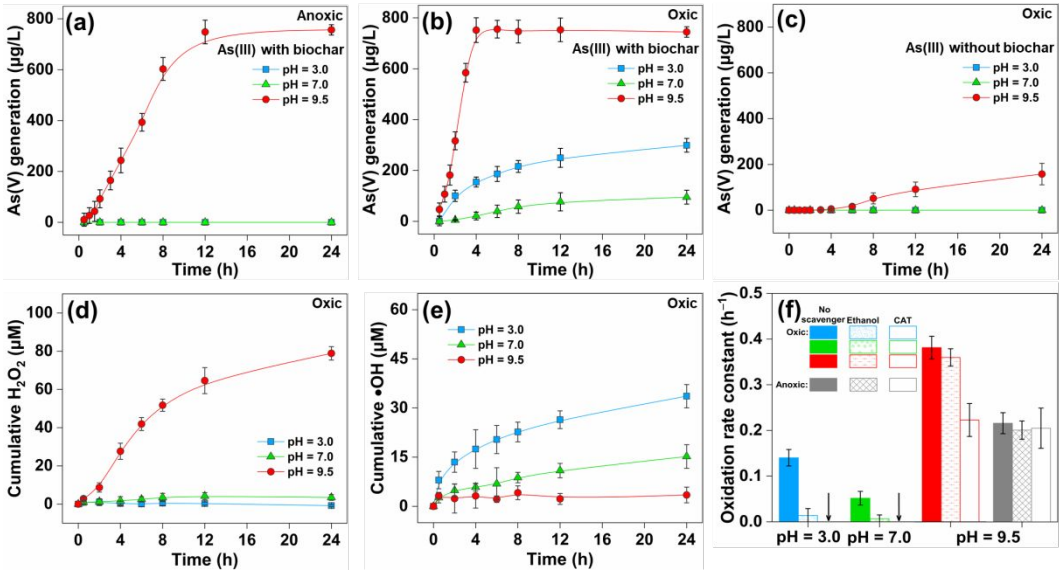

Figure 1. Effect of pH on the oxidation of As(III) to As(V) in the presence of biochar under anoxic (a) and oxic (b) conditions. (c) Effect of pH on the oxidation of As(III) to As(V) in oxic solution without biochar. Cumulative H_2O_2 (d) and •OH (e) generation with biochar under oxic conditions. (f) Effect of ethanol and CAT addition on the As(III) oxidation rate constant in the biochar/As(III) systems. The initial concentrations of BC400, As(III), DMPO, BA, ethanol, and CAT were 2 g/L, 750 μg/L, 100 mM, 10 mM, 50 mM, and 1000 units/mL, respectively; the system pH was maintained at 3.0, 7.0, or 9.5 ± 0.1; the reaction time was set as at 24 h.

Changes in RAMs during As(III) Oxidation. It has been recognized that phenolic –OH, semiquinone-type PFRs, and quinoid C=O on model carbon-based materials (e.g.,

HS and biochar) correspond to the fully reduced, intermediate, and fully oxidized form of quinone structure, respectively, which can reversibly donate and/or accept electrons accompanied with the release and/or consumption of H^+ (Figure S4).[18,22,38] In particular, phenolic –OH and quinoid C=O can act as reductant and oxidant in nitrate reduction and acetate oxidation,[17] respectively, whereas semiquinone-type PFRs can potentially play dual roles in redox transformation of contaminants such as Cr(VI) reduction,[6] As(III) oxidation,[16] and simultaneous reduction and oxidation of *p*-PNP[13] under certain conditions. According to the above literature and our results with As(III) oxidation (Figure 1), RAMs on biochar might play similar roles in As(III) oxidation by direct (e.g., quinoid C=O for As(III) oxidation) and/or indirect (e.g., activation of O_2) pathways, thus leading to their changes. To confirm this, we therefore checked the changes in RAMs before and after the As(III) oxidation.

At pH 9.5, the relative intensity of peak at ~1700 cm^{-1} symbolizing quinoid C=O significantly decreased after the As(III) oxidation (regardless of the presence of O_2), as shown in the FTIR spectra (Figure 2a). High-resolution XPS of O 1s was further employed to explore the change in quinoid C=O before and after the As(III) oxidation (Figure S5a–S5c). The O 1s XPS peak of biochars could be deconvoluted into five oxygen component peaks at 531.1, 532.1, 533.0, 534.1, and 535.2 eV, which were typically assigned to COOH, C=O, C–O–C, C–OH & –OH, and adsorbed H_2O, respectively. The relative area ratio of each component to the O 1s peak is presented in Table S3 and Figure 2b. After the As(III) oxidation, we found that the relative area ratio of quinoid C=O dramatically decreased by 7.9% to 9.6% at pH 9.5, which was

consistent with the FTIR results. These characterization results suggested that quinoid C=O probably accepted electrons from As(III) at pH 9.5. In addition, we observed As(III) oxidation by 1,4-benzoquinone at the same pH value (Figure S6), further validating the direct oxidation of As(III) by quinoid C=O under alkaline conditions. Similarly, PFRs on biochar-derived DOM and HS has been reported to directly oxidize As(III) under alkaline conditions.[16,18] Thus, the EPR technique was applied to investigate changes in PFRs on biochar. Before the As(III) oxidation, biochar exhibited a strong singlet signal, indicating the presence of PFRs on its surface (Figure S7). PFRs with g-factor below 2.0030 are attributed to carbon-centered PFRs, and PFRs with g-factor of 2.0030–2.0040 are attributed to carbon-centered PFRs with an adjacent oxygen atom. In contrast, the g-factor is over 2.0040 for oxygen-centered PFRs.[6] From our results shown in Table S4, the g-factor of PFRs on BC400 was 2.0042, characteristic of oxygen-centered PFRs, namely, semiquinone-type PFRs. After the As(III) oxidation, we found that the concentration of semiquinone-type PFRs markedly decreased from 5.616×10^{17} to 3.277×10^{17} spins/g under oxic conditions and to 3.912×10^{17} spins/g under anoxic conditions (Figure 2c). This observation agreed with a gradual disappearance of the EPR signal of *in situ* generated semiquinone-type PFRs during the excess As(III) oxidation in an alkaline solution (pH 11.0) (Figure S8). In contrast, the control experiments without As(III) showed a slight attenuation of the semiquinone-type PFRs (i.e., 0.852×10^{17} spins/g at pH 3.0, 0.247×10^{17} spins/g at pH 7.0, and 0.555×10^{17} spins/g at pH 9.5) on biochar in anoxic solutions (Figure S7). These results demonstrated that semiquinone-type PFRs may be directly responsible for the

313 As(III) oxidation at pH 9.5 regardless of the presence of O_2. Meanwhile, the decreasing
314 phenolic –OH contents were observed under both oxic and anoxic conditions. These
315 decreases were attributed to the oxidation of phenolic –OH by O_2 and/or the
316 comproportionation (R1) between phenolic –OH and quinoid C=O under alkaline
317 conditions,[39] as corroborated by the increase in semiquinone-type PFRs production at
318 2 h (Figure S9).

319 phenolic –OH + quinoid C = O ↔ semiquinone - type PFRs + H^+ (R1)

320 We noted that the decrease in all RAMs occurred after the As(III) oxidation under
321 alkaline conditions. This seemed to suggest an irreversible transformation of RAMs.
322 Such an irreversible transformation was confirmed by a poorer As(III) oxidation by
323 "reduced" BC400 (collected from the BC400/As(III) system at pH 9.5 under anoxic
324 conditions) than fresh BC400 under acidic and oxic conditions (Figure S10a and Text
325 S8). Two possible explanations for irreversible transformation of RAMs are that: (1)
326 after accepting electrons from As(III), both semiquinone-type PFRs and quinoid C=O
327 possibly transform into new phenolic –OH (different from the indigenous phenolic –
328 OH), which quickly polymerizes under alkaline conditions. It has been reported that
329 under alkaline conditions, phenolic-like substances are prone to polymerize, creating
330 humic acid-like substances.[19,40] After the As(III) oxidation, a higher ratio of C–O–C
331 possibly corresponded to the polymerization of new phenolic –OH produced at pH 9.5,
332 compared with those at pH 3.0 and 7.0 (Table S3 and Figure S5b–S5e); (2) under
333 alkaline and oxic conditions, the newly produced H_2O_2 could attack surface RAMs on
334 biochar, resulting in their irreversible damage due to oxidation, as implied by a higher

concentration of TOC released from biochar in oxic solution than anoxic solution (Figure S11).

At pH 3.0 and 7.0, the relative peak intensities of quinoid C=O were found to have negligible variation under anoxic conditions (Figure S12). Similar to the trend of the change in quinoid C=O, the semiquinone-type PFR concentration remained almost stable in the As(III) solutions after subtracting natural attenuation of semiquinone-type PFRs on BC400 in the As(III)-free solutions (Figure S9). These trends suggested that both quinoid C=O and semiquinone-type PFRs failed to enable As(III) oxidation under acidic-neutral and anoxic conditions, as we observed in Figure 1a. Interestingly, under oxic conditions, the increases in quinoid C=O were clearly observed at pH 3.0 and 7.0 (Table S3, Figure 2a and 2b), but to different extents (3.1% at pH 3.0 vs. 2.5% at pH 7.0). These increases can be illustrated by the oxidative transformation of phenolic –OH and semiquinone-type PFRs to quinoid C=O moieties, as confirmed by the EPR spectra (Figure S7 and Figure 2c) and Boehm titration analyses (Figure 2d). In particular, the semiquinone-type PFR concentration dropped from 5.616×10^{17} to 3.698×10^{17} spins/g at pH 3.0 and to 5.410×10^{17} spins/g at pH 7.0 (Table S4 and Figure 2c). Coinciding with the decrease in the semiquinone-type PFR concentration, the phenolic –OH content decreased from 2.55 to 0.49 mmol/g at pH 3.0, and to 0.83 mmol/g at pH 7.0 (Table S4 and Figure 2d). Furthermore, we found that both the amounts of semiquinone-type PFRs and phenolic –OH consumption were in agreement with the cumulative •OH generation and As(III) oxidation efficiency. These coupled behaviors can be explained by the oxidative transformation process donating electrons

to O_2, which produces $\bullet O_2^-$ and H_2O_2, then •OH (via a successive single-electron transfer reaction) (Figure 1c and 1d), ultimately resulting in the As(III) oxidation (Figure 1b). As shown in Figure S10b, we also found that RAMs on biochar also underwent irreversible transformation during the As(III) oxidation under acidic-neutral and oxic conditions, likely due to the production of ROS for irreversible damages of RAMs (Text S8). Overall, these changes in the RAMs on biochar indicated that they may directly and/or indirectly participate in the As(III) oxidation, and the possible roles of RAMs in the As(III) oxidation will be further illustrated below.

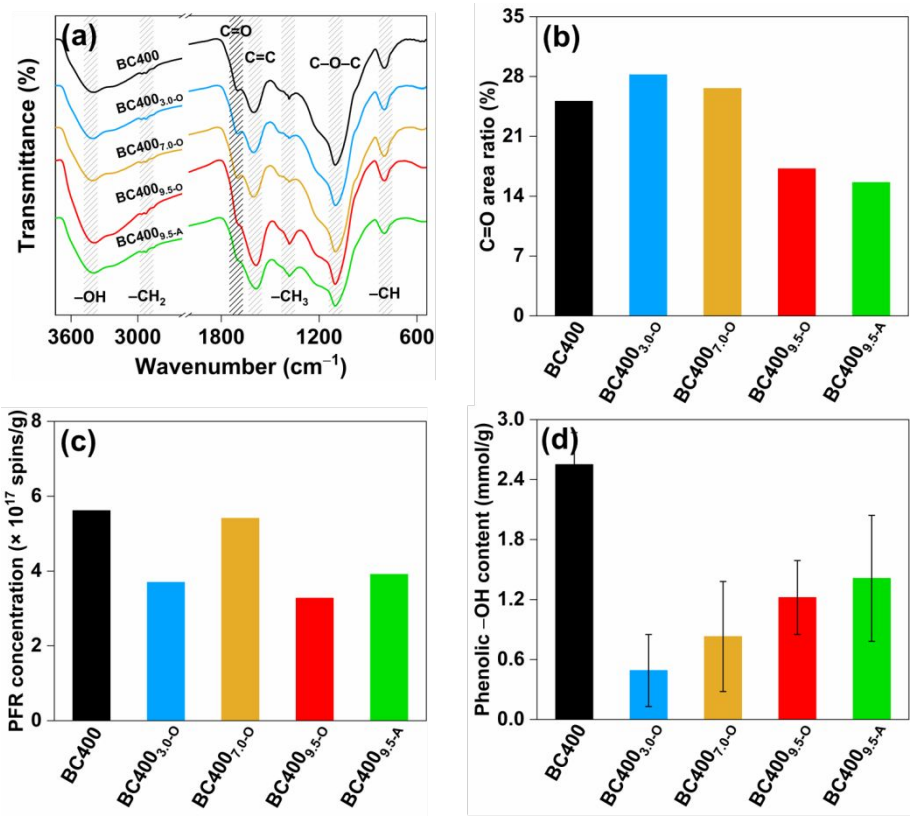

Figure 2. Changes in (a) FTIR spectra, (b) C=O area ratio[a], (c) PFR concentration[b], and (d) phenolic –OH content[c] before and after the As(III) oxidation.

[a] Obtained from the peak area ratio of C=O to the whole peak area based on the O 1s XPS spectra quantitative analysis of selected biochars (Table S3 and Figure S5).

[b] Acquired from EPR analysis of selected biochars (Figure S7).

[c] Determined from a modified Boehm titration (Table S4).

Validation of Reactions with Biochars of Tuned RAM Compositions. A series of biochars with tuned RAM compositions were synthesized and investigated for As(III) oxidation. First, H_2O_2 treatment was used to transform phenolic –OH and semiquinone-type PFRs into quinoid C=O via the aforementioned-electron transfer reactions (Figure S4). From the FTIR spectra shown in Figure 3a, the characteristic peak intensity of quinoid C=O at ~1700 cm^{-1} increased significantly (i.e., oBC400). The O 1s XPS analysis also showed that quinoid C=O increased from 25.1% to 31.1% (Table S3, Figure 3b and S5f). Meanwhile, after the H_2O_2 treatment, both semiquinone-type PFRs and phenolic –OH decreased sharply (Figure 3c and 3d). These results indicated that the transformation of both phenolic –OH and semiquinone-type PFRs into quinoid C=O occurred with the H_2O_2 treatment. It was found that 100% of As(III) was oxidized by oBC400 within 2 h at pH 9.5, which is far higher than that (45.5%) oxidized by BC400 under the same conditions (Figure 4a). Such an accelerated As(III) oxidation was also found under anoxic conditions at pH 9.5 (Figure S13). These results confirmed that quinoid C=O can directly contribute to As(III) oxidation, as corroborated by the FTIR spectral analysis (i.e., a decreasing relative peak intensity of quinoid C=O after As(III) oxidation) (Figure S14). At pH 3.0 and 7.0, however, little As(III) oxidation was observed under oxic conditions (Figure 4b and 4c), because the smaller amounts of phenolic –OH and semiquinone-type PFRs were left to donate electrons to O_2 and to subsequently produce ROS. These were evidenced by the low accumulation of H_2O_2 and •OH (Figure 4e, 4f, 4h, and 4i).

393 Alternatively, KBH_4 treatment was employed to increase the content of phenolic –
394 OH (i.e., rBC400). After the KBH_4 treatment, the phenolic –OH content markedly
395 increased from 2.55 to 5.12 mmol/g, whereas the concentration of semiquinone-type
396 PFRs (g-factor = 2.0042) decreased from 5.616×10^{17} to 3.987×10^{17} spins/g and the ratio
397 of quinoid C=O dropped from 25.1% to 7.3% (Table S3 and S4, and Figure 3a–3d).
398 Specifically, quinoid C=O and semiquinone-type PFRs were successfully reduced to
399 phenolic –OH. In oxic solution at pH 3.0, 55.4% of As(III) was oxidized by rBC400
400 within 24 h, comparing to 39.9% by BC400 (Figure 4b). At pH 7.0, the increase in
401 As(III) oxidation efficiency was similarly observed under oxic conditions (Figure 4c).
402 The results suggested that the increasing phenolic –OH can significantly accelerate the
403 As(III) oxidation under acidic-neutral and oxic conditions, which was attributed to the
404 generation of more ROS from activation of O_2 (Figure 4e, 4f, 4h, and 4i). At pH 9.5,
405 however, the As(III) oxidation by rBC400 was almost equal to that by BC400 (Figure
406 4a and Figure S13), which might be related to *in situ* generated PFRs from the
407 comproportionation between phenolic –OH and quinoid C=O at this pH value, as
408 supported by the small cumulative concentrations of H_2O_2 and •OH (Figure 4d and 4g).
409 In addition, we increased the generation of PFRs by elevating the pyrolysis
410 temperature in the range of 400–500 °C. As shown in Figure 3c and Figure S7, after the
411 500 °C treatment, the PFR concentration increased considerably from 5.616×10^{17} to
412 8.943×10^{17}spins/g. The g-factor of PFRs was 2.0041, corresponding to semiquinone-
413 type PFRs, indicating that the thermal treatment did not change the type of PFRs (Table
414 S4). From the FTIR spectra in Figure 3a, there was a slight increase in the relative peak

intensity at ~1700 cm^{-1} attributed to quinoid C=O, which was also supported by the O 1s XPS analysis (Table S3, Figure 3b and S5h). Nevertheless, it was found that the phenolic –OH obviously declined (Figure 3d). Our results suggested that the thermal treatment markedly removed phenolic –OH, but significantly elevated semiquinone-type PFR concentration. Under oxic conditions, 46.5% and 22.1% of As(III) were oxidized by BC500 at pH 3.0 and 7.0, respectively, higher values than those (39.9% at pH 3.0 and 19.3% at pH 7.0) in the BC400 systems (Figure 3e and 3f). The production of more ROS (e.g., •OH) can explain the enhanced As(III) oxidation by BC500 (Figure 3h and 3i), indicating that semiquinone-type PFRs can be responsible for production of ROS (e.g., •OH) at pH 3.0 and 7.0. At pH 9.5, the promoted As(III) oxidation in the BC500 systems was observed (Figure 4a and Figure S13), though there was a lower concentration of H_2O_2 in the BC500 systems than in the BC400 systems (Figure 4d). The results suggested that semiquinone-type PFRs as electron-accepting moieties can directly oxidize As(III), which agreed with our EPR analysis (Figure S15). Also, these results indicated that semiquinone-type PFRs were much prone to directly oxidize As(III), than activating O_2 to produce ROS for the indirect As(III) oxidation at pH 9.5. Consistent with previous reports,[22] an intermediate heat treatment temperature can elevate both the electron donating and accepting capacities of biochar, resulting in the greater As(III) oxidation by BC500.

To evaluate the significance of the RAMs, we performed a thermal treatment that eliminates RAMs by higher pyrolysis temperature of 800 °C (hereinafter denoted as BC800), and then investigated the oxidation of As(III) by BC800. FTIR spectra

437 demonstrated that the relative peak intensity of quinoid C=O (~1700 cm^{-1}) on BC800
438 was negligible, being much lower than that on BC400 (Figure 3a). This decrease was
439 also confirmed by the O1s XPS analysis (from ~25.1% to ~7.1%) (Table S3, Figure 3b
440 and S5i). After the high-temperature treatment, we found that the PFR concentration
441 fell significantly from 5.616×10^{17} spins/g to below the detection limit (Figure 3c).
442 Similarly, the phenolic –OH content also markedly decreased from 2.55 to 0.12 mmol/g
443 (Table S4 and Figure 3d). These results demonstrated that the high-temperature
444 treatment almost completely removed all RAMs on BC400, which agreed with previous
445 reports.[32,33] As expected, the oxidation of As(III) was significantly suppressed in the
446 presence of BC800 at pH 9.5 (Figure 4a and S13), and almost disappeared at pH 3.0
447 and 7.0 (Figure 4b and 4c). In conclusion, RAMs, i.e., phenolic –OH, semiquinone-
448 type PFRs, and quinoid C=O, played significant roles in the As(III) oxidation.

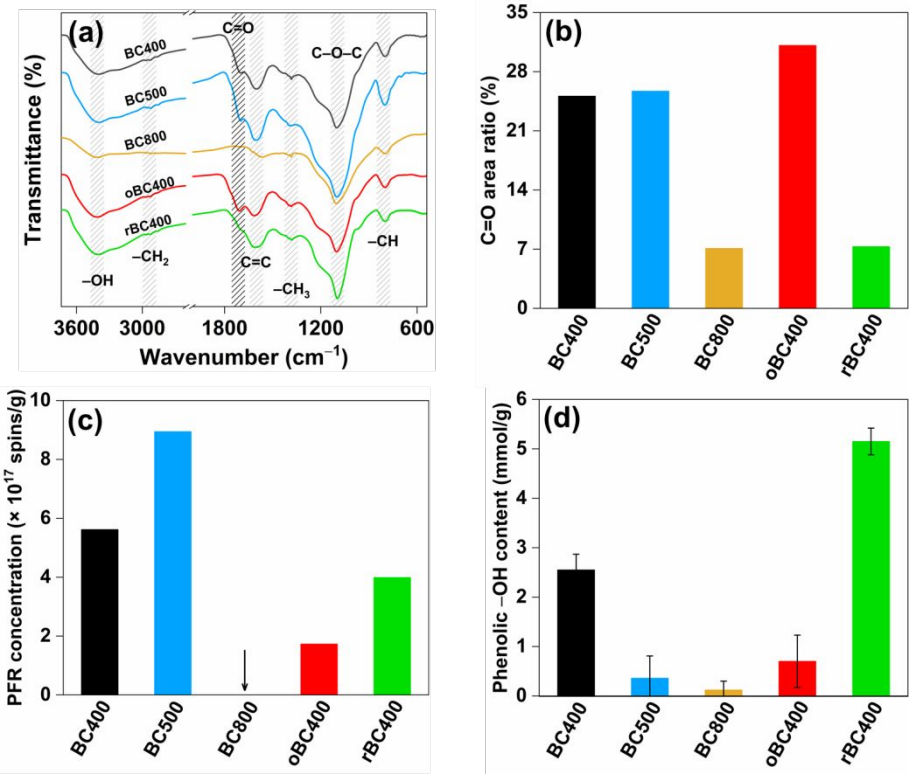

449

450 **Figure 3.** Tuned RAM compositions (a: FTIR spectra; b: C=O area ratio; PFR

concentration; phenolic –OH content) of biochar with different pretreatments.

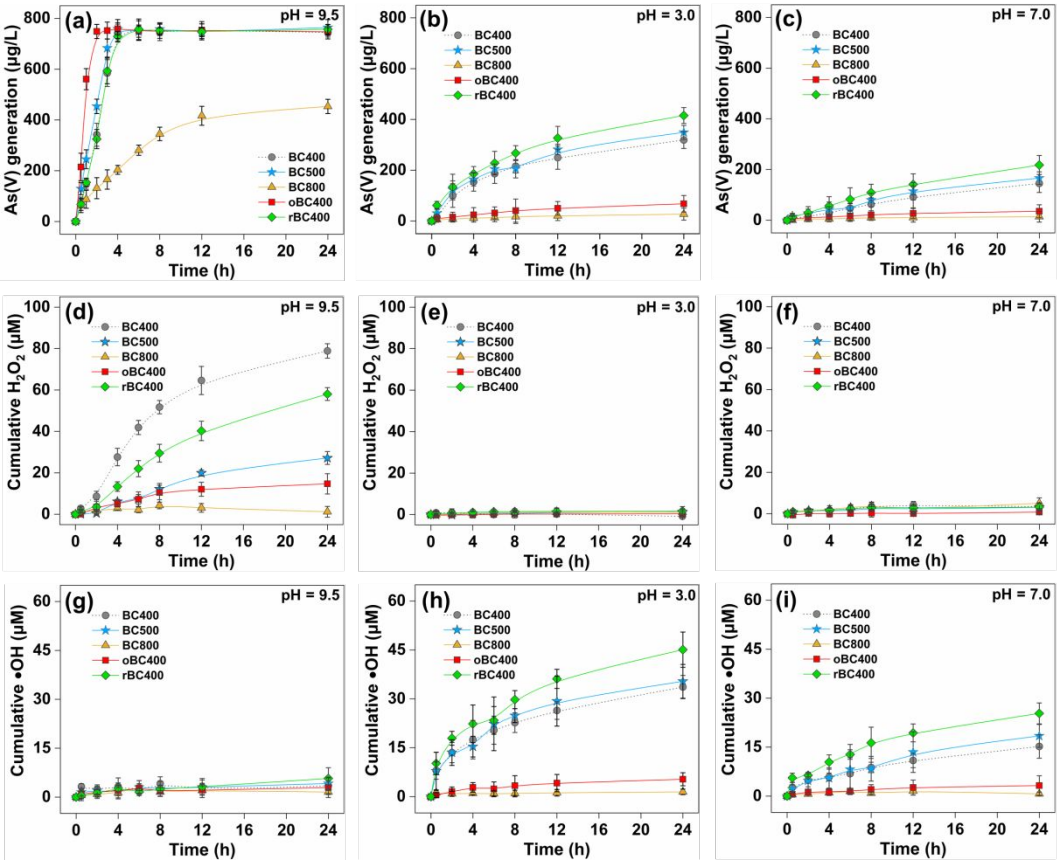

Figure 4. Oxidation of As(III) to As(V) (a–c) and production of cumulative H_2O_2 (d–f), and •OH (g–i) in different biochar (with tuned RAMs compositions) systems under oxic and varying pH conditions. The initial concentrations of biochars, As(III), and BA were 2 g/L, 750 μg/L, and 10 mM, respectively; the system pH was maintained at 3.0, 7.0, or 9.5±0.1; the reaction time was set as at 24 h.

Proposed Mechanisms of As(III) Oxidation. To examine the thermodynamic basis of As(III) oxidation, we first calculated their Eh values at different pH values based on standard reduction potential (Eh) and p*K*a values of As(V)/As(III) (here the occurrence of double-electron transfer reaction (R2) is assumed for simplifying the Eh calculation)[41,42] and the involved ROS redox couples (i.e., O_2/•HO_2 couple, H_2O_2/H_2O couple, and •OH/H_2O couple).[43-45]

$As(V) + 2e^- \rightarrow As(III)$ (R2)

$O_2 + H^+ + e^- = \bullet HO_2$ (R3)

The Eh values of the As(V)/As(III) couple were calculated to be 0.239 V at pH 3.0, –0.122 V at pH 7.0, and –0.397 V at pH 9.5 (Figure S16). In comparison, the Eh values of the $O_2/\bullet HO_2$ couple were –0.021 V at pH 3.0 and –0.127 V at pH 7.0, lower than or close to those of the As(V)/As(III) couple at these two pH values. This can explain our observation that no As(III) oxidation by O_2 occurred under acidic-neutral and oxic conditions (Figure 1c). At pH 9.5, however, the Eh value (–0.127 V) of the $O_2/\bullet HO_2$ couple was far higher than that (–0.397 V) of the As(V)/As(III) couple, accounting for the partial oxidation of As(III) by O_2 (Figure 1c). To date, it is still a great challenge for researchers to collect (conditional) Eh values of $RAMs_{ox}/RAMs_{red}$ (e.g., quinoid C=O/semiquinone-type PFR couple) couples on biochar particles, although efforts have been made toward understanding the structures[46] and the properties (e.g., p*K*a and redox capacity)[22,47] of biochar as well as the development of mediated potentiometry for heterogeneous systems.[48] The exact Eh values of all the specific $RAMs_{ox}/RAMs_{red}$ couples on biochar are mysterious at different pH values, but the apparent bulk Eh values (which were overall reflected by sum of the specific $RAMs_{ox}/RAMs_{red}$ couples on biochar) for the biochar system could be approximately estimated based on our As(III) oxidation and •OH generation from O_2 activation (Figure 1). The apparent bulk Eh values of the $RAMs_{ox}/RAMs_{red}$ couples on biochar would fall below that (–0.021 V at pH 3.0, and –0.127 V at pH 7.0) of the $O_2/\bullet HO_2$ couple in the pH range of 3.0 to 7.0 but would be higher than that (–0.127 V at pH 9.5) of the $O_2/\bullet HO_2$ couple at pH 9.5

(Figure S16). The Eh values would possibly decrease with the pH varying from 3.0 to 7.0, but increase in the pH range of 7.0 to 9.5, which is similar to the Eh-pH diagram for the model HS constructed by Jiang et al..[18] The Eh of the biochar system might be dominantly controlled by the H^+ level at a low pH varying from 3.0 to7.0, but by the ratio of the $RAMs_{ox}/RAMs_{red}$ couples at a high pH 7.0–9.5 due to the appearance of comproportionation (Figure S9). Moreover, the difference between the Eh values of the $RAMs_{ox}/RAMs_{red}$ and the $O_2/•HO_2$ couple at pH 3.0 would be larger than that at pH 7.0 because of the greater amount of •OH production (from activation of O_2 by biochar) at pH 3.0 than that at pH 7.0. The Eh values of the H_2O_2/H_2O and $•OH/H_2O$ couples were much higher than those of the As(V)/As(III) couples in the pH range of 3.0 to 9.5 (Figure S16a), once O_2 was activated by biochar. The results indicated that both H_2O_2 and •OH can directly oxidize As(III) to As(V) at pH 3.0–9.5. The proposed Eh-pH diagrams for the biochar/As(III)/O_2 system possibly reflects the thermodynamic relationship between biochar, As(III), O_2, and the involved ROS in the pH range of 3.0 to 9.5, but needs to be quantified and verified in future investigations.

Recent studies have demonstrated that oxidation of As(III) to As(V) can undergo intermediate and transient As(IV).[44,45,49] Typically, oxidation of As(III) to intermediate and transient As(IV) (E^0(As(IV)/As(III)) = 2.400 V) can be only driven by highly oxidative species via R4 (e.g., •OH, $E^0(•OH/H_2O)$ = 2.730 V), while oxidation of As(IV) to As(V) (E^0(As(V)/As(IV)) = –1.200 V) can be readily driven by a broader range of oxidized species such as O_2 ($E^0(O_2/•HO_2)$ = 0.100 V) and ROS (e.g., •OH) via R5–R6 below.[43,45] In addition to the oxidation of As(III) to As(V) via the successive single-

509 electron transfer reaction, As(III) can be also directly oxidized to As(V) by some
510 oxidants (e.g., H_2O_2) via a double-electron transfer reaction (via R7).[44]

511 $As(III) + \bullet OH + H^+ \rightarrow As(IV) + H_2O$ (R4)

512 $As(IV) + \bullet OH + H^+ \rightarrow As(V) + H_2O$ (R5)

513 $As(IV) + O_2 + H^+ \rightarrow As(V) + \bullet HO_2$ (R6)

514 $As(III) + H_2O_2 + H^+ \rightarrow As(V) + H_2O$ (R7)

515 On the basis of our observations and discussion, the possible mechanisms of As(III)
516 oxidation by biochar under varying pH and O_2 conditions were proposed and illustrated
517 in Scheme 1. Under alkaline conditions, As(III) was initially oxidized to As(IV) (R8
518 and R9) by both semiquinone-type PFRs and quinoid C=O, then further to As(V) by
519 the two moieties (R10 and R11) as well as O_2 (once O_2 was introduced into the systems)
520 (R6). In addition to the above single-electron transfer process for the oxidation As(III)
521 to As(V), the newly produced H_2O_2 can directly oxidize As(III) to As(V) via an
522 additional double-electron transfer reaction under oxic conditions (R7), mainly
523 accounting for O_2-accelerated oxidation of As(III) to As(V) by biochar.

524 As(III) + quinoid C = O → As(IV) + polymers (R8)

525 As(III) + semiquinone - type PFRs → As(IV) + polymers (R9)

526 As(IV) + quinoid C = O → As(V) + polymers (R10)

527 As(IV) + semiquinone - type PFRs → As(V) + polymers (R11)

528 Under acidic-neutral and oxic conditions, both phenolic –OH and semiquinone-type
529 PFRs activated O_2 to form $\bullet HO_2$, and then generated H_2O_2 and •OH via a successive
530 single-electron transfer reaction (R12–R17):

phenolic –OH + O_2 + H^+ → oxidized moieties (semiquinone - type PFRs, quinoid C = O) + $•HO_2$ (R12)

semiquinone - type PFRs + O_2 + H^+ → quinoid C = O + $•HO_2$ (R13)

phenolic –OH + $•HO_2$ + H^+ → oxidized moieties (semiquinone - type PFRs, quinoid C = O) + H_2O_2 (R14)

semiquinone - type PFRs + $•HO_2$ + H^+ → quinoid C = O + H_2O_2 (R15)

phenolic –OH + H_2O_2 → oxidized moieties (semiquinone - type PFRs, quinoid C = O) + •OH + OH^- (R16)

semiquinone - type PFRs + H_2O_2 → quinoid C = O + •OH + OH^- (R17)

The intermediate H_2O_2 directly contributed to slight oxidation of As(III) to As(V) (R7). More importantly, the resulting •OH from activation of H_2O_2 directly accepted electrons from As(III) to produce As(IV) (R4). Subsequent oxidation of As(IV) to As(V) occurred with •OH as well as O_2 (R5 and R6). In summary, biochar indirectly and directly oxidizes As(III) via the above mechanisms at varying pH and O_2 levels.

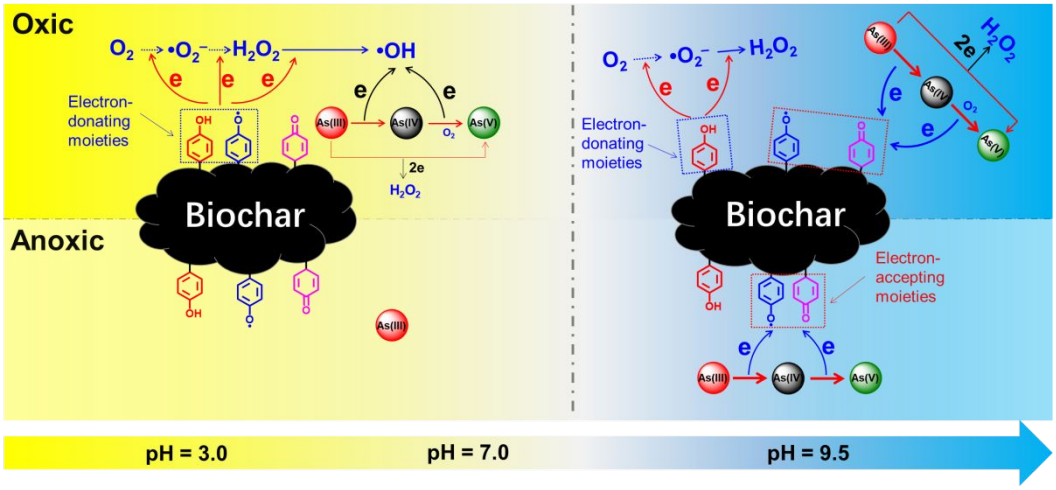

Scheme 1. Mechanisms of pH-dependent As(III) oxidation by biochar.

Environmental Implications. We report that rice-husk-derived biochar directly and indirectly enables As(III) oxidation via different mechanisms at varying pH and O_2 levels, thus mitigating the toxicity and mobility of As. The free radical •OH is generated from oxidation of biochar with electron-donating moieties (i.e., phenolic –OH and

548 PFRs), which occurs only under oxic and acidic-neutral conditions. The generated •OH
549 can non-selectively oxidize trace contaminants in acidic-neutral (waste)water. In
550 alkaline (waste)water, both final product H_2O_2 and biochar with electron-accepting
551 moieties (i.e., PFRs and quinoid C=O) are capable of directly oxidizing trace redox-
552 sensitive contaminants such as As(III). The results of this study shed light on the fact
553 that biochar can be fabricated by design for different purposes involving environmental
554 remediation. This study also paves a possible way to decontaminate trace redox-
555 sensitive metals by other carbonaceous materials such as activated carbon, carbon
556 nanotubes, and graphene oxide. However, it is noted that biochar can potentially release
557 some organic pollutants into aqueous media during the decontamination of trace redox-
558 sensitive metals, elevating its environmental risk (Figure S11). The carbonaceous
559 materials may interact with trace redox-sensitive metals via redox reactions similar to
560 those described herein, thereby altering the transport and fate of the contaminants in
561 aqueous environment.

562 # ASSOCIATED CONTENT

563 **Supporting Information**

564 The Supporting Information is available free of charge on the ACS Publications website
565 at DOI:.

566 Materials and chemicals; preparation of rBC400 and oBC400; data collection and
567 analysis of FTIR, EPR, XPS, and modified Boehm titration; As adsorption
568 analysis; comparison of As(III) oxidation in different systems; proposed Eh-pH
569 diagrams for the biochar/As(III)/O_2 systems.

AUTHOR INFORMATION

Corresponding Authors

*Phone: +86 27 87792159; fax: +86 27 87792101.

E-mail: wanglinling@mail.hust.edu.cn (L. Wang); yanrong_zhang@hust.edu.cn (Y. Zhang).

Notes

The authors declare no competing financial interest.

ACKNOWLEDGEMENTS

This work was supported by the National Natural Science Foundation of China (No. 41671311), State Key Laboratory of Pollution Control and Resource Reuse Foundation (No. PCRRF18027), the National High Technology Research and Development (863) Program of China (No. 2012AA06A304), the China Scholarship Council (No. 201806165010), and Program for HUST Academic Frontier Youth Team (2018QYTD05). The authors would like to thank the Analytical and Testing Center, Huazhong University of Science and Technology, China, for the kind help on sample characterization. We sincerely thank Dr. Rixiang Huang at State University of New York in Albany for the valuable comments.

REFERENCES

(1) Ling, L.-L.; Liu, W.-J.; Zhang, S.; Jiang, H. Magnesium oxide embedded nitrogen self-doped biochar composites: Fast and high-efficiency adsorption of heavy metals in an aqueous solution. *Environ. Sci. Technol.* **2017,** *51*, (17), 10081–10089.

(2) Cao, X.; Ma, L.; Liang, Y.; Gao, B.; Harris, W. Simultaneous immobilization of lead and atrazine in contaminated soils using dairy-manure biochar. *Environ. Sci. Technol.* **2011,** *45*, (11), 4884–4889.

(3) Yao, Y.; Gao, B.; Chen, J.; Yang, L. Engineered biochar reclaiming phosphate from aqueous solutions: Mechanisms and potential application as a slow-release fertilizer. *Environ. Sci. Technol.* **2013,** *47*, (15), 8700–8708.

(4) Woolf, D.; Amonette, J. E.; Street-Perrott, F. A.; Lehmann, J.; Joseph, S. Sustainable biochar to mitigate global climate change. *Nat. Commun.* **2010,** *1*, 56.

(5) Dong, X.; Ma, L. Q.; Zhu, Y.; Li, Y.; Gu, B. Mechanistic investigation of mercury sorption by brazilian pepper biochars of different pyrolytic temperatures based on X-ray photoelectron spectroscopy and flow calorimetry. *Environ. Sci. Technol.* **2013,** *47*, (21), 12156–12164.

(6) Zhong, D.; Zhang, Y.; Wang, L.; Chen, J.; Jiang, Y.; Tsang, D. C. W.; Zhao, Z.; Ren, S.; Liu, Z.; Crittenden, J. C. Mechanistic insights into adsorption and reduction of hexavalent chromium from water using magnetic biochar composite: Key roles of Fe_3O_4 and persistent free radicals. *Environ. Pollut.* **2018,** *243*, 1302–1309.

(7) Chen, B.; Zhou, D.; Zhu, L. Transitional adsorption and partition of nonpolar and polar aromatic contaminants by biochars of pine needles with different pyrolytic temperatures. *Environ. Sci. Technol.* **2008,** *42*, (14), 5137–5143.

(8) Teixidó, M.; Pignatello, J. J.; Beltrán, J. L.; Granados, M.; Peccia, J. Speciation of the ionizable antibiotic sulfamethazine on black carbon (biochar). *Environ. Sci. Technol.* **2011,** *45*, (23), 10020–10027.

(9) Jing, X.-R.; Wang, Y.-Y.; Liu, W.-J.; Wang, Y.-K.; Jiang, H. Enhanced adsorption performance of tetracycline in aqueous solutions by methanol-modified biochar. *Chem. Eng. J.* **2014,** *248*, 168–174.

(10) Fang, Q.; Chen, B.; Lin, Y.; Guan, Y. Aromatic and hydrophobic surfaces of wood-derived biochar enhance perchlorate adsorption via hydrogen bonding to oxygen-containing organic groups. *Environ. Sci. Technol.* **2014,** *48*, (1), 279–288.

(11) Fang, G.; Gao, J.; Liu, C.; Dionysiou, D. D.; Wang, Y.; Zhou, D. Key role of persistent free radicals in hydrogen peroxide activation by biochar: Implications to organic contaminant degradation. *Environ. Sci. Technol.* **2014,** *48*, (3), 1902−1910.

(12) Fang, G.; Zhu, C.; Dionysiou, D. D.; Gao, J.; Zhou, D. Mechanism of hydroxyl radical generation from biochar suspensions: Implications to diethyl phthalate degradation. *Bioresource Technol.* **2015,** *176*, 210–217.

(13) Yang, J.; Pignatello, J. J.; Pan, B.; Xing, B. Degradation of *p*-nitrophenol by lignin and cellulose chars: H_2O_2-mediated reaction and direct reaction with the char. *Environ. Sci. Technol.* **2017,** *51*, (16), 8972–8980.

(14) Gehling, W.; Dellinger, B. Environmentally persistent free radicals and their lifetimes in $PM_{2.5}$. *Environ. Sci. Technol.* **2013,** *47*, (15), 8172–8178.

(15) Yang, J.; Pan, B.; Li, H.; Liao, S.; Zhang, D.; Wu, M.; Xing, B. Degradation of *p*-nitrophenol on biochars: Role of persistent free radicals. *Environ. Sci. Technol.* **2016,** *50*, (2), 694–700.
(16) Dong, X.; Ma, L. Q.; Gress, J.; Harris, W.; Li, Y. Enhanced Cr(VI) reduction and As(III) oxidation in ice phase: Important role of dissolved organic matter from biochar. *J. Hazard. Mater.* **2014,** *267*, 62−70.
(17) Saquing, J. M.; Yu, Y.-H.; Chiu, P. C. Wood-derived black carbon (biochar) as a microbial electron donor and acceptor. *Environ. Sci. Technol. Let.* **2016,** *3*, (2), 62–66.
(18) Jiang, J.; Bauer, I.; Paul, A.; Kappler, A. Arsenic redox changes by microbially and chemically formed semiquinone radicals and hydroquinones in a humic substance model quinone. *Environ. Sci. Technol.* **2009,** *43*, (10), 3639–3645.
(19) Qin, W.; Wang, Y.; Fang, G.; Wu, T.; Liu, C.; Zhou, D. Evidence for the generation of reactive oxygen species from hydroquinone and benzoquinone: Roles in arsenite oxidation. *Chemosphere* **2016,** *150*, 71–78.
(20) Qin, W.; Wang, Y.; Fang, G.; Liu, C.; Sui, Y.; Zhou, D. Oxidation mechanism of As(III) in the presence of polyphenols: New insights into the reactive oxygen species. *Chem. Eng. J.* **2016,** *285*, 69–76.
(21) Wang, L.; Cho, D.-W.; Tsang, D. C. W.; Cao, X.; Hou, D.; Shen, Z.; Alessi, D. S.; Ok, Y. S.; Poon, C. S. Green remediation of As and Pb contaminated soil using cement-free clay-based stabilization/solidification. *Environ. Int.* **2019,** *126*, 336–345.
(22) Klüpfel, L.; Keiluweit, M.; Kleber, M.; Sander, M. Redox properties of pant biomass-derived black carbon (biochar). *Environ. Sci. Technol.* **2014,** *48*, (10), 5601–5611.
(23) Wu, S.; Fang, G.; Wang, Y.; Zheng, Y.; Wang, C.; Zhao, F.; Jaisi, D. P.; Zhou, D. Redox-active oxygen-containing functional groups in activated carbon facilitate microbial reduction of ferrihydrite. *Environ. Sci. Technol.* **2017,** *51*, (17), 9709–9717.
(24) Lou, L.; Liu, F.; Yue, Q.; Chen, F.; Yang, Q.; Hu, B.; Chen, Y. Influence of humic acid on the sorption of pentachlorophenol by aged sediment amended with rice-straw biochar. *Appl. Geochem.* **2013,** *33*, 76–83.
(25) Niazi, N. K.; Bibi, I.; Shahid, M.; Ok, Y. S.; Burton, E. D.; Wang, H.; Shaheen, S. M.; Rinklebe, J.; Lüttge, A. Arsenic removal by Perilla leaf biochar in aqueous solutions and groundwater: An integrated spectroscopic and microscopic examination. *Environ. Pollut.* **2018,** *232*, 31–41.
(26) Niazi, N. K.; Bibi, I.; Shahid, M.; Ok, Y. S.; Shaheen, S. M.; Rinklebe, J.; Wang, H.; Murtaza, B.; Islam, E.; Farrakh Nawaz, M.; Lüttge, A. Arsenic removal by Japanese Oak wood biochar in aqueous solutions and well water: Investigating arsenic fate using integrated spectroscopic and microscopic techniques. *Sci. Total Environ.* **2018,** *621*, 1642–1651.
(27) Mariner, P. E.; Holzmer, F. J.; Jackson, R. E.; Meinardus, H. W.; Wolf, F. G. Effects of high pH on arsenic mobility in a shallow sandy aquifer and on aquifer permeability along the adjacent shoreline, commencement bay superfund site, Tacoma, Washington. *Environ. Sci. Technol.* **1996,** *30*, (5), 1645–1651.
(28) Fakhreddine, S.; Dittmar, J.; Phipps, D.; Dadakis, J.; Fendorf, S. Geochemical triggers of arsenic mobilization during managed aquifer recharge. *Environ. Sci. Technol.*

2015, *49*, (13), 7802–7809.
(29) Tang, L.; Feng, H.; Tang, J.; Zeng, G.; Deng, Y.; Wang, J.; Liu, Y.; Zhou, Y. Treatment of arsenic in acid wastewater and river sediment by Fe@Fe_2O_3 nanobunches: The effect of environmental conditions and reaction mechanism. *Water Res.* **2017,** *117*, 175–186.
(30) Guo, H.; Wen, D.; Liu, Z.; Jia, Y.; Guo, Q. A review of high arsenic groundwater in mainland and Taiwan, China: Distribution, characteristics and geochemical processes. *Appl. Geochem.* **2014,** *41*, 196–217.
(31) Qin, Y.; Zhang, L.; An, T. Hydrothermal carbon-mediated Fenton-like reaction mechanism in the degradation of alachlor: Direct electron transfer from hydrothermal carbon to Fe(III). *ACS Appl. Mater. Inter.* **2017,** *9*, (20), 17115–17124.
(32) Chen, N.; Huang, Y.; Hou, X.; Ai, Z.; Zhang, L. Photochemistry of hydrochar: Reactive oxygen species generation and sulfadimidine degradation. *Environ. Sci. Technol.* **2017,** *51*, (19), 11278–11287.
(33) Fang, G.; Liu, C.; Gao, J.; Dionysiou, D. D.; Zhou, D. Manipulation of persistent free radicals in biochar to activate persulfate for contaminant degradation. *Environ. Sci. Technol.* **2015,** *49*, 5645−5653.
(34) Uchimiya, M.; Lima, I. M.; Thomas Klasson, K.; Chang, S.; Wartelle, L. H.; Rodgers, J. E. Immobilization of heavy metal Ions (Cu^{II}, Cd^{II}, Ni^{II}, and Pb^{II}) by broiler litter-derived biochars in water and soil. *J. Agr. Food Chem.* **2010,** *58*, (9), 5538–5544.
(35) Balmer, M. E.; Sulzberger, B. Atrazine degradation in irradiated iron/oxalate systems: Effects of pH and oxalate. *Environ. Sci. Technol.* **1999,** *33*, (14), 2418–2424.
(36) Tong, M.; Yuan, S.; Ma, S.; Jin, M.; Liu, D.; Cheng, D.; Liu, X.; Gan, Y.; Wang, Y. Production of abundant hydroxyl radicals from oxygenation of subsurface sediments. *Environ. Sci. Technol.* **2016,** *50*, (1), 214–221.
(37) Khachatryan, L.; Vejerano, E.; Lomnicki, S.; Dellinger, B. Environmentally persistent free radicals (EPFRs). 1. generation of reactive oxygen species in aqueous solutions. *Environ. Sci. Technol.* **2011,** *45*, (19), 8559–8566.
(38) Uchimiya, M.; Stone, A. T. Redox reactions between iron and quinones: Thermodynamic constraints. *Geochim. Cosmochim. Acta* **2006,** *70*, (6), 1388–1401.
(39) Uchimiya, M.; Stone, A. T. Reversible redox chemistry of quinones: Impact on biogeochemical cycles. *Chemosphere* **2009,** *77*, (4), 451–458.
(40) Sadykh-Zade, S. I.; Ragimov, A. V.; Suleimanova, S. S.; Liogon'kii, V. I. The polymerization of quinones in an alkaline medium and the structure of the resulting polymers. *Polymers Sci. U.S.S.R.* **1972,** *14*, (6), 1395–1403.
(41) Renock, D.; Voorhis, J. Electrochemical investigation of arsenic redox processes on pyrite. *Environ. Sci. Technol.* **2017,** *51*, (7), 3733–3741.
(42) Willianl P. Inskeep, T. R. M., Scott Fendorf, Arsenic(V)/(III) cycling in soils and natural waters: Chemical and microbiological processes. In *Environmental Chemistry of Arsenic*, William T. Frankenberger, J., Ed. Marcel Dekker, Inc.: New York, 2001; pp 183–215.
(43) Koppenol, W. H.; Stanbury, D. M.; Bounds, P. L. Electrode potentials of partially reduced oxygen species, from dioxygen to water. *Free Radical Bio. Med.* **2010,** *49*, (3), 317–322.

(44) Kim, D.-h.; Bokare, A. D.; Koo, M. s.; Choi, W. Heterogeneous catalytic oxidation of As(III) on nonferrous metal oxides in the presence of H_2O_2. *Environ. Sci. Technol.* **2015,** *49*, (6), 3506–3513.
(45) Chen, Z.; Jin, J.; Song, X.; Zhang, G.; Zhang, S. Redox conversion of arsenite and nitrate in the UV/quinone systems. *Environ. Sci. Technol.* **2018,** *52*, (17), 10011–10018.
(46) Xiao, X.; Chen, B. A direct observation of the fine aromatic clusters and molecular structures of biochars. *Environ. Sci. Technol.* **2017,** *51*, (10), 5473–5482.
(47) Chen, Z.; Xiao, X.; Chen, B.; Zhu, L. Quantification of chemical states, dissociation constants and contents of oxygen-containing groups on the surface of biochars produced at different temperatures. *Environ. Sci. Technol.* **2015,** *49*, (1), 309–317.
(48) Gorski, C. A.; Edwards, R.; Sander, M.; Hofstetter, T. B.; Stewart, S. M. Thermodynamic characterization of iron oxide–aqueous Fe^{2+} redox couples. *Environ. Sci. Technol.* **2016,** *50*, (16), 8538–8547.
(49) Sun, M.; Zhang, G.; Qin, Y.; Cao, M.; Liu, Y.; Li, J.; Qu, J.; Liu, H. Redox conversion of chromium(VI) and arsenic(III) with the intermediates of chromium(V) and arsenic(IV) via AuPd/CNTs electrocatalysis in acid aqueous solution. *Environ. Sci. Technol.* **2015,** *49*, (15), 9289–9297.

TOC Art